



Deposited via The University of Leeds.

White Rose Research Online URL for this paper:

<https://eprints.whiterose.ac.uk/id/eprint/119263/>

Version: Accepted Version

---

**Article:**

Hua, Y, Jonnalagadda, R, Zhang, L et al. (2017) Assessment of general and localized corrosion behavior of X65 and 13Cr steels in water-saturated supercritical CO<sub>2</sub> environments with SO<sub>2</sub>/O<sub>2</sub>. International Journal of Greenhouse Gas Control, 64. pp. 126-136. ISSN: 1750-5836

<https://doi.org/10.1016/j.ijggc.2017.07.012>

---

© 2017 Published by Elsevier Ltd. Licensed under the Creative Commons Attribution-NonCommercial-NoDerivatives 4.0 International <http://creativecommons.org/licenses/by-nc-nd/4.0/>

**Reuse**

Items deposited in White Rose Research Online are protected by copyright, with all rights reserved unless indicated otherwise. They may be downloaded and/or printed for private study, or other acts as permitted by national copyright laws. The publisher or other rights holders may allow further reproduction and re-use of the full text version. This is indicated by the licence information on the White Rose Research Online record for the item.

**Takedown**

If you consider content in White Rose Research Online to be in breach of UK law, please notify us by emailing [eprints@whiterose.ac.uk](mailto:eprints@whiterose.ac.uk) including the URL of the record and the reason for the withdrawal request.

1 **Assessment of general and localized corrosion behavior of X65 and 13Cr steels in water-**  
2 **saturated supercritical CO<sub>2</sub> environments with SO<sub>2</sub>/O<sub>2</sub>**

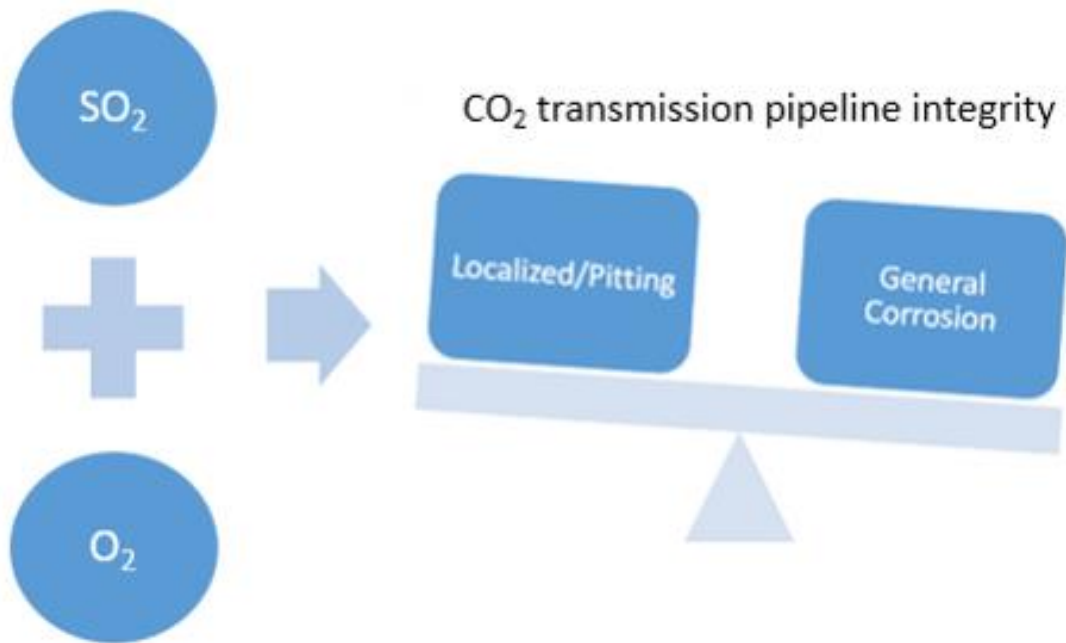
3  
4 Yong Hua<sup>\*a</sup>, Raghu Jonnalagadda<sup>a</sup>, Lei Zhang<sup>b</sup>, Anne Neville<sup>a</sup> and Richard Barker<sup>a</sup>

5  
6 <sup>a</sup> Institute of Functional Surfaces, School of Mechanical Engineering, University of Leeds,  
7 Leeds, LS2 9JT, UK

8 <sup>b</sup> Corrosion and Protection Centre, University of Science and Technology Beijing, 30 Xueyuan  
9 Road, Beijing, China

10  
11 \*Corresponding author: Yong Hua, Tel: 07923359918, Email: [leo.huayong@gmail.com](mailto:leo.huayong@gmail.com)

12



13

14

**Abstract**

15 To mitigate the corrosive effect encountered in carbon steel pipelines during dense phase CO<sub>2</sub>  
16 transport the general consensus is that the CO<sub>2</sub> stream must be sufficiently dehydrated.  
17 Although such a process will undoubtedly help prevent the breakout of free water, it can  
18 contribute significantly towards the handling costs, particularly in the context of offshore  
19 installations. As opposed to drying the CO<sub>2</sub> stream to excessive levels, one alternative option

20 is the application of corrosion resistant alloys such as 13Cr. This paper performs a comparison  
21 between X65 carbon steel and 13Cr in pure and impure CO<sub>2</sub>, evaluating the influence of SO<sub>2</sub>  
22 and O<sub>2</sub> on the general and localized corrosion rate of both materials at 80 bar and 35°C. The  
23 results show that 13Cr is able to perform exceptionally well in comparison to X65 in pure CO<sub>2</sub>  
24 as well as when SO<sub>2</sub> and O<sub>2</sub> are present in the system individually, producing no localized  
25 corrosion and general corrosion rates below 0.02 mm/y. However, when SO<sub>2</sub> and O<sub>2</sub> were  
26 combined, the formation of sulfuric acid was permitted which proved detrimental to 13Cr,  
27 producing excessive localized attack much greater than that observed on X65. Raman  
28 spectroscopy, XRD and SEM/EDX are used to analyse the corrosion products

29 **Key words:** CO<sub>2</sub> corrosion, carbon steel, carbon capture and storage, sulfur dioxide, oxygen

## 30 **1. Introduction**

31 Fossil fuels will continue to be the dominant source of the world's energy production for the  
32 foreseeable future, yet there has been increased concern that the combustion of such carbon-  
33 based fuels produces greenhouse gases (particularly CO<sub>2</sub>), which adversely affect the global  
34 climate.<sup>[1]</sup>

35 The implementation of Carbon Capture and Storage (CCS) technology would allow the  
36 continued use of fossil fuels through the abatement of carbon dioxide (CO<sub>2</sub>), preventing  
37 emissions into the atmosphere. Currently, CCS is the only process available to generate a  
38 significant and immediate impact on the Earth's environment.

39 CCS refers to a process by which CO<sub>2</sub> is captured from large point sources (e.g. power  
40 generation and industrial applications), followed by compression and transportation to a  
41 storage site (e.g. a geological reservoir or depleted oil field). For the transmission of large

42 quantities of CO<sub>2</sub>, the most logical and cost effective solution would be the development of a  
43 dedicated pipeline network manufactured from carbon steel to transport CO<sub>2</sub> in a liquid or  
44 supercritical state. However, one limitation of carbon steel is its susceptibility to corrosion in  
45 flue gas environments due to the presence of CO<sub>2</sub>, water (H<sub>2</sub>O), oxygen (O<sub>2</sub>), sulfur dioxide  
46 (SO<sub>2</sub>), nitrogen oxides (NO<sub>x</sub>) and other constituents that can result in the formation of  
47 corrosive phases.

48 A number of studies have recently been published which seek to understand the implications  
49 of such impurities in liquid or supercritical CO<sub>2</sub> on the extent of carbon steel corrosion during  
50 pipeline transportation.<sup>[2-20]</sup> Research has also focused on defining the safe limits of impurities  
51 that can be tolerated within the CO<sub>2</sub> stream by systematically varying the water content or  
52 concentration of other contaminants such as SO<sub>2</sub>, O<sub>2</sub> and NO<sub>x</sub> amongst others.<sup>[4, 5, 7, 9, 18, 20, 33,</sup>  
53 <sup>34, 35, 36]</sup>

54 From a review of the literature within this subject area it appears that in order to  
55 appropriately mitigate excessive corrosion rates the general consensus is that sufficient  
56 drying (i.e. water removal) of impure CO<sub>2</sub> upstream of the pipeline is required. Although such  
57 a process can prevent the breakout of free water, it can contribute significantly towards  
58 handling costs, particularly in the context of offshore installations.<sup>[1]</sup> Furthermore, some  
59 studies have suggested that extensive dehydration down to 50 ppm (mole) should be applied,  
60 which can require the use of molecular sieves, imposing an even greater cost<sup>[9, 32]</sup>. Limits as  
61 low as 50 ppm have already been implemented in the US<sup>[21]</sup> and Norway<sup>[22]</sup> for specific  
62 pipelines. However, other specifications from the DYNAMIS project<sup>[23]</sup> and for the Kinder  
63 Morgan pipeline<sup>[24]</sup> are less conservative, imposing limits of 500 and 650 ppm, respectively.

64 As opposed to dehydrating the CO<sub>2</sub> stream, one alternative option is the application of  
65 corrosion resistant alloys (CRAs) such as 13Cr. However, limited data on CRA corrosion in  
66 dense phase CO<sub>2</sub> is available in the literature with the exception of work by Choi et al.<sup>[16]</sup> which  
67 was performed with 13Cr in the presence of very high SO<sub>2</sub>/O<sub>2</sub> concentrations (1% and 5%,  
68 respectively) that are orders of magnitude greater than those typically anticipated for  
69 anthropogenic CO<sub>2</sub> transport according to Walspurger et al.<sup>[25]</sup>.

70 The purpose of this present study is to contribute to the literature by determining the ability  
71 of 13Cr relative to X65 carbon steel to mitigate corrosion in water-saturated dense phase CO<sub>2</sub>  
72 when SO<sub>2</sub> and O<sub>2</sub> are present both individually and together. Both the general and localized  
73 corrosion behavior of X65 and 13Cr are determined using white light interferometry and the  
74 nature and morphology of corrosion products formed on the steel surface are reviewed using  
75 a combination of scanning electron microscopy (SEM), energy dispersive X-ray spectroscopy  
76 (EDX), and X-ray diffraction (XRD) in order to clarify the role low concentrations of SO<sub>2</sub> and O<sub>2</sub>  
77 play in the degradation process and ascertain whether selection of a CRA is a suitable  
78 corrosion mitigation option.

## 79 **2. Experimental procedure**

### 80 **2.1 Sample preparation**

81 Test specimens were machined into discs of diameter 25 mm and thickness of 6 mm from  
82 both API 5L X65 carbon steel and 13Cr (UNS41000) bars. The chemical composition of X65  
83 and 13Cr and their microstructures are provided in Table 1 and Figure 1 respectively. Surface  
84 preparation for corrosion experiments consisted of wet-grinding the entire sample with up to  
85 600 grit silicon carbide abrasive paper, rinsing with distilled water, followed by acetone and  
86 high purity ethanol, followed by drying gently with compressed air. Samples were then stored

87 in a desiccator until required and weighed immediately before the experiment on an  
88 electronic balance to within an accuracy of 0.01 mg before suspending inside the autoclave.  
89 Two samples of the same material were placed within the autoclave for each individual test.  
90 Surface preparation for the microstructures consisted of wet-grinding the entire sample  
91 surface up to 1200 grit silicon carbide abrasive paper, followed by polishing with the help of  
92 3 $\mu$ m diamond suspension to attain a mirror finish, rinsing with distilled water, followed by  
93 acetone, high purity ethanol and drying gently with compressed air. Etchants were varied  
94 depending on the sample alloy composition. A 2% Nital was used for X65 where etching  
95 consisted of swabbing the surface for 10-20 seconds with a cotton pad. 13Cr was etched with  
96 waterless Kalling's reagent (5 g copper chloride + 100 ml hydrochloric acid + 100 ml ethanol)  
97 by swabbing the surface for 10 seconds with a cotton pad.

98

## 99 **2.2 Autoclave testing procedure**

100 A schematic representation of the autoclave experimental system layout is provided in Figure  
101 2. The testing procedure has been published in a previous paper. <sup>[7]</sup>

102 All tests were conducted under static conditions in water-saturated supercritical CO<sub>2</sub> (a water  
103 content of 3437 ppm in the dense phase at 80 bar and 35°C based on the analysis performed  
104 by Spycher et al.<sup>[26]</sup>). However, in order to ensure complete saturation of CO<sub>2</sub> under these  
105 conditions, 34000 ppm of water was introduced to the bottom of the autoclave (i.e. not in  
106 direct contact with the sample). The entire matrix of the experimental conditions is provided  
107 in Table 2 which describes the different materials and conditions that were evaluated. The  
108 molar concentrations of SO<sub>2</sub> (100 ppm) and O<sub>2</sub> (1000 ppm) were specifically chosen to reflect  
109 the recommended limits proposed by de Visser et al.<sup>[23]</sup> and Alstom (which can be found in a

110 publication by Dugstad et al.<sup>[13]</sup>) to ensure safe CO<sub>2</sub> transport. However, it should be noted  
111 that the proposed limits within these publications are based on health and safety criteria in  
112 the event of a sudden release from a pipeline, not from the perspective of corrosion/pipeline  
113 integrity. This study aims to evaluate whether these proposed limits are tolerable within a  
114 CO<sub>2</sub> pipeline when the stream is saturated with water. Previous research <sup>[37, 38]</sup> has indicated  
115 that the addition of these particular impurities at the aforementioned concentrations do not  
116 shift the critical point of CO<sub>2</sub> significantly. As such, all experiments performed in this study are  
117 conducted with CO<sub>2</sub> within its supercritical state.

118 It is difficult to monitor the actual pH of the solution due to the presence of small amounts of  
119 water in the system and the considerable pressure. Consequently, the OLI software <sup>[31]</sup> was  
120 used to speculate about the possible pH of the aqueous phase as shown in Figure 3.  
121 Considering the experimental conditions in this work (35°C and 80 bar CO<sub>2</sub>), the solution pH  
122 is expected to reduce from 3.1 in the absence of SO<sub>2</sub> to 2.4 when 100 ppm SO<sub>2</sub> is introduced.  
123 This is based on the assumption that SO<sub>2</sub> will partially dissolve into the aqueous phase to form  
124 sulfurous acid (H<sub>2</sub>SO<sub>3</sub>) as stated by Dugstad et al.<sup>[10]</sup> It is difficult to predict the effect of  
125 combined addition of O<sub>2</sub> and SO<sub>2</sub> to this system. However, based on the assumption that the  
126 likely effect is to promote the formation of sulfuric acid through the oxidation of sulfurous  
127 acid, the pH can be expected to decrease markedly given that sulfuric acid is a much stronger  
128 acid.

129 At the end of each experiment, the specimens were dried thoroughly and subsequently  
130 chemically cleaned to remove all traces of corrosion products before weighing. The cleaning  
131 process consisted of wiping the surface with a cotton pad soaked in Clarke's solution (20 g  
132 antimony trioxide + 50 g stannous chloride + 1000 ml hydrochloric acid) in accordance with

133 ASTM Standard G1-03<sup>[27]</sup>. This was followed by rinsing the samples with distilled water and  
134 then drying with compressed air.

135 The mass loss due to corrosion was determined from the weight difference before exposure  
136 and after cleaning. The corrosion rates were calculated using Equation (1):

$$V_c = \frac{87600\Delta m}{\rho A t} \quad (1)$$

137 where  $V_c$  is the corrosion rate of the sample in mm/year,  $\Delta m$  is the weight loss in grams,  $\rho$  is  
138 the density of the sample in g/cm<sup>3</sup>,  $A$  is the exposed area in cm<sup>2</sup> and  $t$  is the immersion time  
139 in hours.

### 140 **3. Results and Discussion**

#### 141 **3.1 General corrosion of X65 and 13Cr steels exposed to water-saturated supercritical CO<sub>2</sub>** 142 **condition with various SO<sub>2</sub>/O<sub>2</sub> concentrations**

143 Figure 4 provides the general corrosion rates recorded (based on gravimetric analysis) for X65  
144 and 13Cr exposed to water-saturated conditions in the presence of various concentrations of  
145 SO<sub>2</sub> and O<sub>2</sub>. In the absence of SO<sub>2</sub> and O<sub>2</sub>, the general corrosion rates of X65 and 13Cr are 0.1  
146 and 0.003 mm/y, respectively. Addition of 1000 ppm O<sub>2</sub> serves to reduce the general  
147 corrosion rates of both materials to 0.03 and 0.001 mm/year. The ability of O<sub>2</sub> to reduce the  
148 general corrosion of carbon steel in CO<sub>2</sub> systems has been reported previously by other  
149 authors at low temperatures and can be attributed to the formation of protective oxide films  
150 on the steel surface<sup>[5, 28]</sup>. In terms of 13Cr, O<sub>2</sub> is also known to assist in the formation and  
151 replenishment of the passive chromium oxide films that can be established on the steel  
152 surface, which can explain the increase in general corrosion resistance with the introduction  
153 of O<sub>2</sub>.

154 The mass loss measurements in Figure 4 indicate that O<sub>2</sub> has no detrimental effect on the  
155 general corrosion of X65 and 13Cr in a CO<sub>2</sub>-H<sub>2</sub>O-O<sub>2</sub> system under these particular conditions  
156 and that 13Cr exhibits improved corrosion resistance compared to X65 in both environments .  
157 The superiority of 13Cr relative to X65 in CO<sub>2</sub>-H<sub>2</sub>O and CO<sub>2</sub>-H<sub>2</sub>O-O<sub>2</sub> systems at high pressure  
158 was also reported by Choi et al.<sup>[16]</sup> for experiments performed at 80 bar and 50°C in CO<sub>2</sub>-  
159 saturated water. However, in contrast to the results in Figure 4, Choi et al.<sup>[16]</sup> reported an  
160 increase in general corrosion rates of X65 for experiments in water-saturated CO<sub>2</sub> with the  
161 introduction of O<sub>2</sub>. A possible explanation for the disparity in observations could be linked to  
162 the temperature difference in experiments, but also the higher O<sub>2</sub> contents of 1.6-5.5 bar  
163 evaluated by Choi et al.,<sup>[16]</sup>. As O<sub>2</sub> content and temperature are increased, O<sub>2</sub> is capable of  
164 influencing the kinetics of the cathodic reaction at the steel surface (see Equation (2) for the  
165 reaction under acidic environments), which may explain the accelerated corrosion reported  
166 by Choi and co-workers.<sup>[16]</sup>



167

168 Referring again to Figure 4, the introduction of solely 100 ppm SO<sub>2</sub> to the CO<sub>2</sub> system resulted  
169 in an increase in general corrosion rates of X65 and 13Cr from 0.1 and 0.003 mm/y to 0.65  
170 and 0.01 mm/y, respectively. Generally, the acceptable internal corrosion limit for such  
171 pipelines is ~0.1 mm/y, although this depends on the system design life and the anticipated  
172 corrosivity of the fluid being transported. For the sake of material evaluation, adopting 0.1  
173 mm/y as an acceptable benchmark, the corrosion rate of X65 under these conditions is well  
174 beyond this limit, whereas 13Cr is still able to offer adequate corrosion protection even in a  
175 water-saturated environment.

176 Addition of both 100 ppm SO<sub>2</sub> and 1000 ppm O<sub>2</sub> (final column in Figure 4) clearly enhances  
177 the corrosion rate of both materials from the pure CO<sub>2</sub> environment, particularly in the case  
178 of 13Cr. The general corrosion rates recorded were 0.95 and 0.75 mm/y for X65 and 13Cr,  
179 respectively. The collection of results within Figure 4 indicate a noticeable synergistic effect  
180 between SO<sub>2</sub> and O<sub>2</sub>. Corrosion rates observed when SO<sub>2</sub> and O<sub>2</sub> are together exceed the sum  
181 of the two individual degradation rates when the both species are present individually. The  
182 observed synergistic effect is evident in both materials and results in 13Cr exceeding 0.1  
183 mm/y by a large margin (by 0.65 mm/year), making it an unsuitable material choice for such  
184 an environment based on this reported limit.

### 185 **3.2 Corrosion product morphology for X65**

186 Figure 5 shows the SEM images of the X65 steel surface after 48 h exposure to the water-  
187 saturated CO<sub>2</sub> phase containing different concentrations of SO<sub>2</sub> and O<sub>2</sub>. In the absence of SO<sub>2</sub>  
188 and O<sub>2</sub>, iron carbonate (FeCO<sub>3</sub>) is the sole crystalline product recorded on the steel surface  
189 (Figure 5(a)) and this is confirmed by the XRD pattern provided in Figure 6. Addition of 1000  
190 ppm O<sub>2</sub> inhibited the formation of FeCO<sub>3</sub>, producing a seemingly amorphous corrosion  
191 product layer which produced no XRD pattern within Figure 6. XPS analysis of the film in a  
192 previous publication identified that the film formed under these conditions predominantly  
193 comprises of iron oxides and/or hydroxides<sup>[5]</sup>. It is assumed that the oxidation of Fe<sup>2+</sup> to Fe<sup>3+</sup>  
194 due to the presence of O<sub>2</sub> inhibits the formation of FeCO<sub>3</sub>.

195 Addition of solely 100 ppm SO<sub>2</sub> (SEM image in Figure 5(c)) produced a corrosion product layer  
196 comprising of both FeCO<sub>3</sub> and iron sulfite (FeSO<sub>3</sub>) according to the XRD pattern provided in  
197 Figure 6. This was confirmed by additional Raman spectroscopy measurements performed on  
198 the same sample. The introduction of both 100 ppm SO<sub>2</sub> and 1000 ppm O<sub>2</sub> resulted in the

199 formation of  $\text{FeCO}_3$  and  $\text{FeSO}_3$  (confirmed by XRD patterns in Figure 6), but also the co-  
200 presence of hydrated  $\text{FeSO}_4$  based on localized Raman spectra (specifically peaks at 185, 480  
201 and  $990\text{ cm}^{-1}$ <sup>[29]</sup> identified within Figure 7).

202 These observations are in alignment with Choi et al.<sup>[16]</sup> who reported that the presence of  $\text{SO}_2$   
203 alone promoted the formation of  $\text{FeSO}_3$  on X65 steel while the addition of  $\text{O}_2$  can form  $\text{FeSO}_4$ .  
204 The work is also in alignment with Dugstad et al.<sup>[10]</sup> who stated that the presence of  $\text{SO}_2$   
205 permits the formation of sulfurous acid ( $\text{H}_2\text{SO}_3$ ), and the addition of  $\text{O}_2$  enables sulfuric acid  
206 ( $\text{H}_2\text{SO}_4$ ) to be formed via the series of reactions (3) to (5).  $\text{H}_2\text{SO}_4$  is a significantly stronger acid  
207 than  $\text{H}_2\text{SO}_3$ , and is potentially more corrosive, corroborating with the observed synergistic  
208 effect between  $\text{O}_2$  and  $\text{SO}_2$ .



209 The formation of sulfite and sulfate ions enables the precipitation of  $\text{FeSO}_3$  and  $\text{FeSO}_4$  via  
210 precipitation reactions:



211 while  $\text{FeCO}_3$  is produced from the precipitation of iron and bicarbonate ions formed from the  
212 steel dissolution and dissociation of carbonic acid within the aqueous phase:



### 213 3.3 Corrosion product morphology for 13Cr

214 13Cr samples exposed to 0 ppm SO<sub>2</sub> with and without 1000 ppm O<sub>2</sub> produced general  
215 corrosion rates below 0.003 mm/year, indicating that O<sub>2</sub> presence has little effect on the  
216 general corrosion of the CRA. SEM images of the steel surface indicated no noticeable signs  
217 of general or localized corrosion and are provided in Figure 8. SEM images of the 13Cr surface  
218 after exposure to 100 ppm SO<sub>2</sub> with and without 1000 ppm O<sub>2</sub> are provided in Figure 9 and  
219 show clear signs of material degradation as a result of introducing SO<sub>2</sub>, the presence of SO<sub>2</sub>  
220 permits the formation of H<sub>2</sub>SO<sub>3</sub> and the addition of O<sub>2</sub> enables H<sub>2</sub>SO<sub>4</sub> to be formed. Both  
221 H<sub>2</sub>SO<sub>3</sub> and H<sub>2</sub>SO<sub>4</sub> are more corrosive in comparison to that of H<sub>2</sub>CO<sub>3</sub>, corroborating with the  
222 increased mass loss observed. No significant corrosion product was visible on the 13Cr surface  
223 exposed to solely 100 ppm SO<sub>2</sub> (Figure 9(a)) as degradation rates under these conditions were  
224 still low at 0.01 mm/y and unlikely to result in substantial corrosion product precipitation.  
225 However, the combined presence of SO<sub>2</sub> and O<sub>2</sub> resulted in corrosion rates rising to 0.65  
226 mm/y, producing a thin, cracked corrosion product layer (Figure 9(b)).

227 XRD and Raman analysis of the corrosion product observed in the SEM image shown in Figure  
228 9(b) proved challenging and were unable to identify the nature of the corrosion product  
229 present. However, cross-section EDX analysis of the films formed on X65 and 13Cr after  
230 exposure to 100 ppm SO<sub>2</sub> and 1000 ppm O<sub>2</sub> after 6 h and 48 h (Figure 10) showed that the  
231 thickness of the corrosion products increased for both materials and the corrosion product  
232 on 13Cr was rich in Cr, S and O, and contained very little traces of Fe. Given that the combined  
233 presence of O<sub>2</sub> and SO<sub>2</sub> permits the formation of H<sub>2</sub>SO<sub>4</sub>, as discussed by Dugstad et al.<sup>[10]</sup>, it is  
234 suggested that this acid is capable of dissolving the Cr<sub>2</sub>O<sub>3</sub> passive film and reacting with Cr<sup>3+</sup>

235 to produce chromium sulfate ( $\text{Cr}_2(\text{SO}_4)_3$ ), although this cannot be confirmed and requires  
236 further study.

237

### 238 **3.4 Localized corrosion of X65 and 13Cr**

239 One particular concern in acidic environments, particularly in CRAs is the potential for  
240 localized corrosion to occur. Each material and test environment combination considered in  
241 Figure 1 (and Table 2) was evaluated for localized attack using white-light interferometry. The  
242 threshold value used was  $1\ \mu\text{m}$  and so the measured localized depth beneath that value of  
243 depth will not be considered. An example of profilometry images of X65 and 13Cr sample  
244 surface exposure to water-saturated  $\text{CO}_2$  condition in the presence of 100 ppm  $\text{SO}_2$  and 1000  
245 ppm  $\text{O}_2$  are provided in Figure 11. Smaller versions of these images are also embedded within  
246 Figure 12 which provides a summary of the pit/localized depth measurements extracted from  
247 X65 and 13Cr samples from all tests performed in Figure 1 and are expressed as penetration  
248 rates. The localized/pit depth analysis was conducted in alignment with ASTM Standard G46-  
249 94, selecting the average of the 10 deepest pits on the surface to provide an accurate  
250 assessment<sup>[30]</sup>. Multiple scans (at least 3) such as those shown in Figure 11 were performed  
251 across the steel surface to ensure reliable data was obtained.

252 Considering Figure 12, it is evident that X65 steel undergoes localized attack in all  
253 environments. The attack manifests itself as a form of micro-pitting over 48 h (typical image  
254 shown in Figure 11) and is particularly prominent in the presence of 1000 ppm  $\text{O}_2$  and 100  
255 ppm  $\text{SO}_2$ /1000 ppm  $\text{O}_2$ , exceeding pitting rates of 2 mm/year. In contrast, 13Cr was only  
256 susceptible to localized corrosion when both  $\text{SO}_2$  and  $\text{O}_2$  were present together. Under these  
257 conditions, the form of corrosion observed was a combination of extensive localized attack

258 and pitting, with the surrounding material adjacent to the attack undergoing significantly less  
259 attack. SEM images of the X65 and 13Cr surfaces after 6h and 48 h of exposure are provided  
260 in Figure 13. These images were taken after cleaning with Clarke's solution and etching the  
261 steel surface; they indicate that the pit initiation is not limited to solely the ferrite phase of  
262 the material for X65 steel.

### 263 **3.5 100 ppm SO<sub>2</sub> and 1000 ppm O<sub>2</sub> – evolution of corrosion products and general/localized** 264 **corrosion rate vs time**

265 The initial localized depth measurements at 48 h in the previous section cast ambiguity over  
266 the actual growth of pits/localized areas as they are purely one measurement performed at a  
267 particular instance in time. To determine the nature of surface pit growth/rate of localized  
268 attack, X65 and 13Cr samples were exposed to the 100 ppm SO<sub>2</sub>/1000 ppm O<sub>2</sub> environment  
269 for varying exposure times between 6 and 48 h. After each experiment, gravimetric  
270 measurements and surface profilometry were performed on both materials to determine the  
271 general and localized corrosion rates, respectively. The data collected is provided in Figure 14  
272 and shows that there is little difference between the general corrosion rate of X65 and 13Cr  
273 over 48 h of exposure. However, a difference of one order of magnitude is recorded between  
274 X65 and 13Cr in terms of localized attack, with 13Cr showing much greater susceptibility to  
275 the SO<sub>2</sub>/O<sub>2</sub> environment than X65 steel. Both materials display decay in their rate of localized  
276 attack as a function of time. The actual general and localized corrosion rates could be higher  
277 than the values recorded here due to depletion of impurities in a closed autoclave over time.  
278 However, the localized attack for both materials remain high for the duration of the  
279 experiment.

280 The evolution of corrosion products on the surface of X65 and 13Cr is provided in Figure 15  
281 and indicates the presence of a sulfur-rich, cracked film as early as 6 h into the experiment on  
282 both materials. Further work is still needed to determine when exactly pit nucleation starts  
283 to occur and what causes this process. Additionally, further work is required to determine  
284 whether the reduction in localized corrosion rate is attributed to corrosion product formation  
285 in the localized region, re-passivation of the oxide film or depletion of impurities within the  
286 autoclave.

### 287 **Conclusions**

288 The research presented has focused towards studying and quantifying the extent of both  
289 general and localized corrosion of X65 and 13Cr in water-saturated supercritical CO<sub>2</sub>  
290 environments containing various SO<sub>2</sub> and O<sub>2</sub>, representative of dense phase CO<sub>2</sub> transport.  
291 Tests were conducted at a pressure of 80 bar and a temperature of 35°C for periods of up to  
292 48 h. The main conclusions which can be drawn from this study are:

- 293 • The general and localized corrosion rate of X65 in water-saturated dense-phase  
294 environments is accentuated by the presence of 100 ppm SO<sub>2</sub> and 100 ppm SO<sub>2</sub>/1000  
295 ppm O<sub>2</sub>. The effect of 1000 ppm O<sub>2</sub> as a sole impurity served to reduce general  
296 corrosion rates, but promotes more substantial pitting on the steel surface.
- 297 • The most aggressive environment for X65 was obtained when SO<sub>2</sub> and O<sub>2</sub> were  
298 combined together which produced general corrosion rates of 0.95 mm/y. SO<sub>2</sub> alone  
299 in the water-saturated dense phase CO<sub>2</sub> permits the formation of sulfurous acid,  
300 which resulted in the precipitation of FeSO<sub>3</sub> on the steel surface. However, the  
301 addition of O<sub>2</sub> was shown to result in the formation of SO<sub>4</sub><sup>2-</sup> (through the formation of  
302 sulphuric acid), producing FeSO<sub>4</sub> on the steel surface.
- 303 • 13Cr was shown to be highly resistant to corrosion in the CO<sub>2</sub>-H<sub>2</sub>O-O<sub>2</sub> and CO<sub>2</sub>-H<sub>2</sub>O  
304 environments, producing no indication of localized attack and general corrosion rates  
305 below 0.003 mm/y. The material also performed well in experiments with 100 ppm  
306 SO<sub>2</sub> present, producing no signs of localized corrosion and general corrosion rates  
307 below 0.02 mm/y.

- 308 • The combined presence of O<sub>2</sub> and SO<sub>2</sub> was detrimental to 13Cr, producing general  
309 corrosion rates of 0.65 mm/y. A clear synergistic effect was observed between SO<sub>2</sub>  
310 and O<sub>2</sub> for both X65 and 13Cr whereby the degradation rates resulting from the  
311 combined presence exceeded the total of the corrosion rates produced when the  
312 species were present individually.
- 313 • Pitting rates of X65 and 13Cr were shown to be in excess of 7 and 80 mm/year at the  
314 start of the experiment for X65 and 13Cr, respectively. The pitting rates were shown  
315 to reduce with time by around an order of magnitude. It was not clear whether the  
316 reduction in corrosion rate was attributed to corrosion product formation, pit  
317 repassivation or depletion of impurities within the system.

318

## 319 **References**

- 320 1. G.A. Jacobson, S. Kerman, Y.-S. Choi, A. Dugstad, S. Nesic, and S. Papavinasam, "Pipeline  
321 Corrosion Issues Related to Carbon Capture, Transportation, and Storage", *Materials*  
322 *Performance*, (2014): p. 24-31.
- 323 2. Y. Hua, R. Barker, and A. Neville, "Comparison of corrosion behaviour for X-65 carbon steel in  
324 supercritical CO<sub>2</sub>-saturated water and water-saturated/unsaturated supercritical CO<sub>2</sub>", *The*  
325 *Journal Of Supercritical Fluids*, 97, (2015): p. 224-237.
- 326 3. Y. Hua, R. Barker, and A. Neville, "Relating iron carbonate morphology to corrosion  
327 characteristics for water-saturated supercritical CO<sub>2</sub> systems", *The Journal Of Supercritical*  
328 *Fluids*, 98, (2015).
- 329 4. Y. Hua, R. Barker, and A. Neville, "The influence of SO<sub>2</sub> on the tolerable water content to avoid  
330 pipeline corrosion during the transportation of supercritical CO<sub>2</sub>", *International Journal of*  
331 *Greenhouse Gas Control*, 37, (2015): p. 412-423.
- 332 5. Y. Hua, R. Barker, and A. Neville, "The effect of O<sub>2</sub> content on the corrosion behaviour of X65  
333 and 5Cr in water-containing supercritical CO<sub>2</sub> environments", *Applied Surface Science*, 356,  
334 (2015): p. 499-511.

- 335 6. Y. Hua, R. Barker, and A. Neville, "Effect of temperature on the critical water content for  
336 general and localised corrosion of X65 carbon steel in the transport of supercritical CO<sub>2</sub>",  
337 International Journal of Greenhouse Gas Control, 31, (2014): p. 48-60.
- 338 7. Y. Hua, R. Barker, and A. Neville, "Understanding the influence of SO<sub>2</sub> and O<sub>2</sub> on the corrosion  
339 of carbon steel in water-saturated supercritical CO<sub>2</sub>", Corrosion, 71, 5 (2014): p. 667-683.
- 340 8. M. Halseid, A. Dugstad, and B. Morland, "Corrosion and bulk phase reactions in CO<sub>2</sub> transport  
341 pipelines with impurities: Review of recent published studies", Energy Procedia, 63, (2014): p.  
342 2557-2569.
- 343 9. J. Brown, B. Graver, E. Gulbrandsen, A. Dugstad, and B. Morland, "Update of DNV  
344 Recommended Practice RP-J202 with focus on CO<sub>2</sub> corrosion with impurities", Energy  
345 Procedia, 63, (2014): p. 2432-2441.
- 346 10. A. Dugstad, M. Halseid, and B. Morland, "Effect of SO<sub>2</sub> and NO<sub>2</sub> on corrosion and solid  
347 formation in dense phase CO<sub>2</sub> pipelines", Energy Procedia, 37, (2013): p. 2877-2887.
- 348 11. A. Dugstad, M. Halseid, B. Morland, and A.O. Sivertsen, "Corrosion in dense phase CO<sub>2</sub> – the  
349 impact of depressurisation and accumulation of impurities", Energy Procedia, 37, 0 (2013): p.  
350 3057-3067.
- 351 12. A. Dugstad, B. Morland, and S. Clausen, "Corrosion of transport pipelines for CO<sub>2</sub> - Effect of  
352 water ingress", Energy Procedia, 4, (2011): p. 3063-3070.
- 353 13. A. Dugstad, S. Clausen, and B. Morland. "Transport of dense phase CO<sub>2</sub> in C-steel pipelines -  
354 when is corrosion an issue?", CORROSION 2011, paper no. 70, (Houston, TX:NACE, 2011).
- 355 14. Y.-S. Choi, S. Hassani, T.N. Vu, and S. Nesic. "Effect of H<sub>2</sub>S on the corrosion behavior of pipeline  
356 steels in supercritical and liquid CO<sub>2</sub> environments", CORROSION 2015, paper no. 5927,  
357 (Dallas, TX: NACE, 2015).
- 358 15. S. Sim, I.S. Cole, Y.S. Choi, and N. Birbilis, "A review of the protection strategies against internal  
359 corrosion for the safe transport of supercritical CO<sub>2</sub> via steel pipelines for CCS purposes",  
360 International Journal of Greenhouse Gas Control, 29, (2014): p. 185-199.

- 361 16. Y.-S. Choi, S. Nešić, and D. Young, "Effect of impurities on the corrosion behavior of CO<sub>2</sub>  
362 transmission pipeline steel in supercritical CO<sub>2</sub>-water environments", *Environmental Science  
363 & Technology*, 44, 23 (2010): p. 9233-9238.
- 364 17. Y. Xiang, Z. Wang, Z. Li, and W. Ni, "Effect of temperature on corrosion behaviour of X70 steel  
365 in high pressure CO<sub>2</sub>/SO<sub>2</sub>/O<sub>2</sub>/H<sub>2</sub>O environments", *Corrosion Engineering, Science and  
366 Technology*, 48, 2 (2013): p. 121-129.
- 367 18. Y. Xiang, Z. Wang, X. Yang, Z. Li, and W. Ni, "The upper limit of moisture content for  
368 supercritical CO<sub>2</sub> pipeline transport", *The Journal of Supercritical Fluids*, 67, (2012): p. 14-21.
- 369 19. Y. Xiang, Z. Wang, Z. Li, and W.D. Ni, "Effect of Exposure Time on the Corrosion Rates of X70  
370 Steel in Supercritical CO<sub>2</sub>/SO<sub>2</sub>/O<sub>2</sub>/H<sub>2</sub>O Environments", *Corrosion*, 69, 3 (2012): p. 251-258.
- 371 20. Y. Xiang, Z. Wang, C. Xu, C. Zhou, Z. Li, and W. Ni, "Impact of SO<sub>2</sub> concentration on the  
372 corrosion rate of X70 steel and iron in water-saturated supercritical CO<sub>2</sub> mixed with SO<sub>2</sub>", *The  
373 Journal of Supercritical Fluids*, 58, 2 (2011): p. 286-294.
- 374 21. F.W. Schremp and G.R. Roberson, "Effect of supercritical carbon dioxide (CO<sub>2</sub>) on construction  
375 materials", *SPE*, 15, 3 (1975): p. 227-233.
- 376 22. A. Oosterkamp and J. Ramsen, "State-of-the-art overview of CO<sub>2</sub> pipeline transport with  
377 relevance to offshore pipelines", *Polytech Report No: POL-O-2007-138-A*, (2008).
- 378 23. E. de Visser, C. Hendriks, M. Barrio, M.J. MølInvik, G. de Koeijer, S. Liljemark, and Y. Le Gallo,  
379 "Dynamis CO<sub>2</sub> quality recommendations", *International Journal of Greenhouse Gas Control*, 2,  
380 4 (2008): p. 478-484.
- 381 24. Kinder Morgan, "CO<sub>2</sub> Transportation pipelines", [Online], Available at:  
382 <http://www.kindermorgan.com/business/co2/transport.cfm>. Accessed on 11th March 2015.
- 383 25. S. Walspurger and H.A.J.v. Dijk, "EDGAR CO<sub>2</sub> purity: type and quantities of impurities related  
384 to CO<sub>2</sub> point source and capture technology: a literature study", *ECN-E-12-054*, (2012).

- 385 26. N. Spycher, K. Pruess, and J. Ennis-King, "CO<sub>2</sub>-H<sub>2</sub>O mixtures in the geological sequestration of  
386 CO<sub>2</sub>. I. Assessment and calculation of mutual solubilities from 12 to 100°C and up to 600 bar",  
387 Geochimica et Cosmochimica Acta, 67, 16 (2003): p. 3015-3031.
- 388 27. ASTM, Standard G1-03, Standard practice for preparing, cleaning, and evaluating corrosion  
389 test specimens. ASTM International: West Conshohocken, PA, 2003.
- 390 28. G. Schmitt and R. Forster. "Unexpected Effect of Small Oxygen Concentrations in Sales Gas on  
391 Element Currents between Pipeline Steel and Magnetite from Black Powder", CORROSION  
392 2015: NACE International, 2015).
- 393 29. C.H. Chio, S.K. Sharma, and D.W. Muenow, "The hydrates and deuterates of ferrous sulfate  
394 (FeSO<sub>4</sub>): a Raman spectroscopic study", Journal of Raman Spectroscopy, 38, 1 (2007): p. 87-  
395 99.
- 396 30. ASTM, Standard G46-94, Standard guide for examination and evaluation of pitting corrosion.  
397 ASTM International: West Conshohocken, PA, 2003.
- 398 31. OLI is a commercial software package from Corr Science, for more information see:  
399 <http://www.corrscience.com/products/oli/>.
- 400 32. R. Barker, Y. Hua, and A. Neville, Internal corrosion of carbon steel pipelines for dense -phase  
401 CO<sub>2</sub> transport in carbon capture and storage (CCS)—a review. International Materials Reviews,  
402 2017. **62**(1): p. 1-31.
- 403 33. Xu, M., Q. Zhang, X. Yang, Z. Wang, J. Liu, and Z. Li, *Impact of surface roughness and humidity*  
404 *on X70 steel corrosion in supercritical CO<sub>2</sub> mixture with SO<sub>2</sub>, H<sub>2</sub>O, and O<sub>2</sub>*. The Journal of  
405 Supercritical Fluids, 2016. **107**: p. 286-297.
- 406 34. Sun, C., J. Sun, Y. Wang, X. Lin, X. Li, X. Cheng, and H. Liu, Synergistic effect of O<sub>2</sub>, H<sub>2</sub>S and SO<sub>2</sub>  
407 impurities on the corrosion behavior of X65 steel in water-saturated supercritical CO<sub>2</sub> system.  
408 Corrosion Science, 2016.

- 409 35. Sun, J., C. Sun, G. Zhang, X. Li, W. Zhao, T. Jiang, H. Liu, X. Cheng, and Y. Wang, Effect of O<sub>2</sub>  
410 and H<sub>2</sub>S impurities on the corrosion behavior of X65 steel in water-saturated supercritical CO<sub>2</sub>  
411 system. *Corrosion Science*, 2016. **107**: p. 31-40.
- 412 36. Sun, C., Y. Wang, J. Sun, X. Lin, X. Li, H. Liu, and X. Cheng, Effect of impurity on the corrosion  
413 behavior of X65 steel in water-saturated supercritical CO<sub>2</sub> system. *The Journal of Supercritical*  
414 *Fluids*, 2016. **116**: p. 70-82.
- 415 37. Farelas. F, Choi. Y.-S., and Nešić. S, Corrosion Behavior of API 5L X65 Carbon Steel  
416 under Supercritical and Liquid Carbon Dioxide Phases in the Presence of Water and  
417 Sulfur Dioxide. *Corrosion*, 2012. **69**(3): p. 243-250.
- 418 38. Farelas. F, Choi Y.-S., and Nesic. S, "Effects of CO<sub>2</sub> phase change, SO<sub>2</sub> content and flow  
419 on the corrosion of CO<sub>2</sub> transmission pipeline steel", in *CORROSION 2012*. 2012: Salt  
420 Lake City, UT:NACE.

421

422

**Table 1: Elemental composition (wt.%) of API 5L X65 carbon steel and UNS41000 13Cr**

	<b>X65</b>	<b>13Cr</b>
C	0.12	0.15
Si	0.18	0.36
Mn	1.27	0.56
P	0.008	0.006
S	0.002	0.008
Cr	0.11	13.5
Mo	0.17	-
Fe	Balance	

423

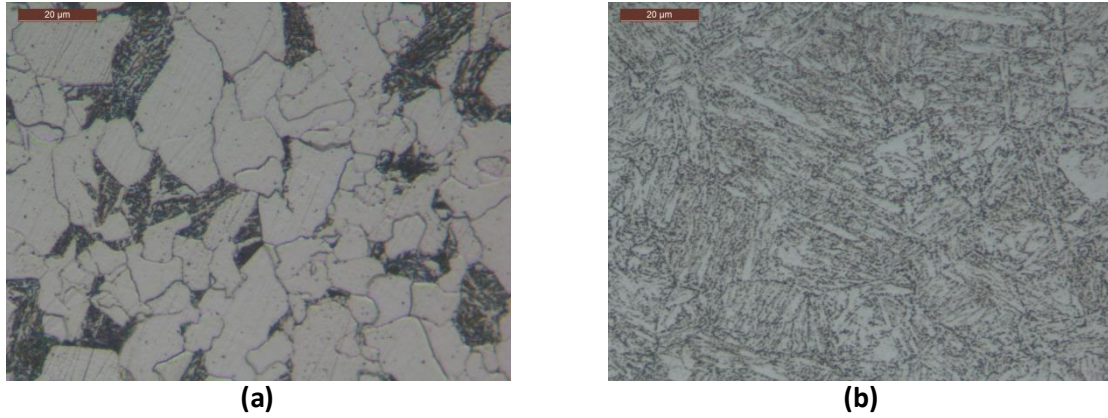
424

**Table 2: Test matrix for corrosion experiments in water-saturated dense phase CO<sub>2</sub>**

<b>Temperature (°C)</b>	<b>Pressure (bar)</b>	<b>Materials</b>	<b>H<sub>2</sub>O (ppm)</b>	<b>SO<sub>2</sub> (ppm)</b>	<b>O<sub>2</sub> (ppm)</b>	<b>Immersion time hours</b>
35	80	X65/13Cr	Above solubility limit of 3437ppm through addition of 34000ppm water	0	0	48
				0	1000	
				100	0	
				100	1000	
<b>Temperature (°C)</b>	<b>Pressure (bar)</b>	<b>Materials</b>	<b>H<sub>2</sub>O (ppm)</b>	<b>SO<sub>2</sub> (ppm)</b>	<b>O<sub>2</sub> (ppm)</b>	<b>Immersion time hours</b>
35	80	X65/13Cr	Above solubility limit of 3437ppm through addition of 34000ppm water	100	1000	6/14/24/48

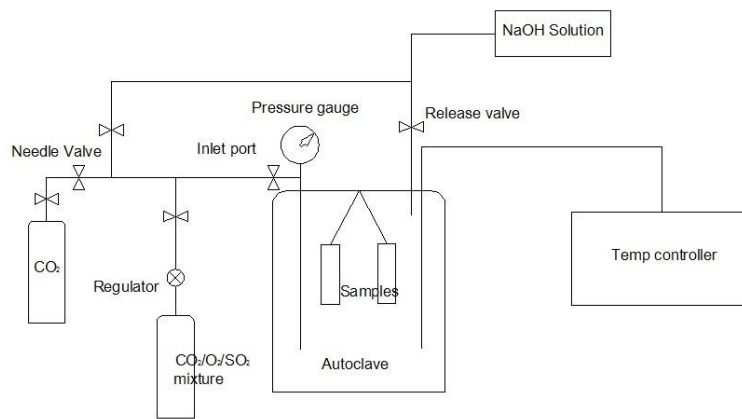
425

426



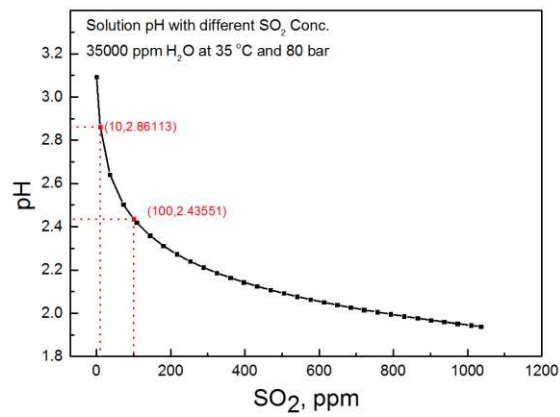
427 **Figure 1: Microstructure of a) API 5L X65 – depicting a ferritic-pearlitic structure and b) UNS41000**  
428 **13Cr – depicting a martensitic structure**

429

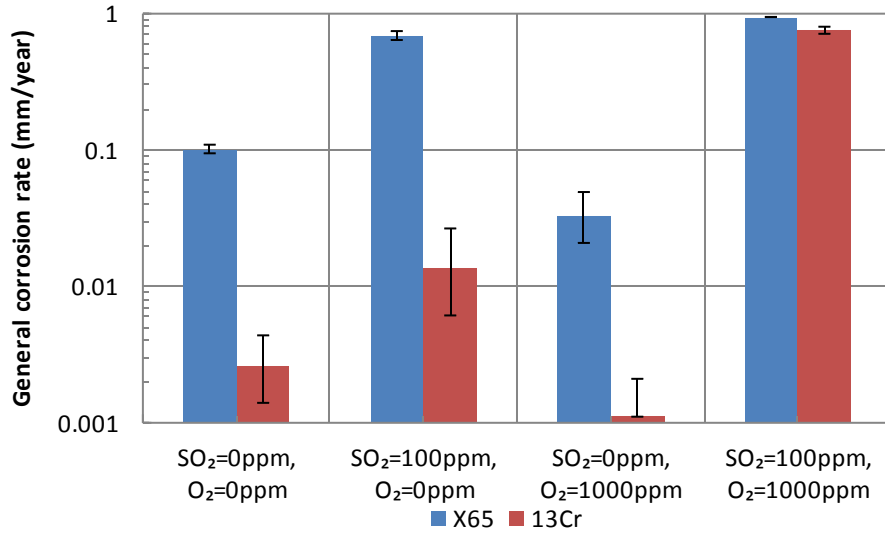


430 **Figure 2: Schematic of the autoclave setup for impure, dense phase CO<sub>2</sub> experiments**

431



432 **Figure 3: Predicted pH of CO<sub>2</sub>-saturated water in the presence of SO<sub>2</sub> at 35°C and 80 bar**



433

434

**Figure 4: General corrosion rates of X65 and 13Cr after exposure to water-saturated dense phase CO<sub>2</sub> at 80 bar and 35 °C for 48 h in the presence of various concentrations of SO<sub>2</sub> and O<sub>2</sub>**

435

436

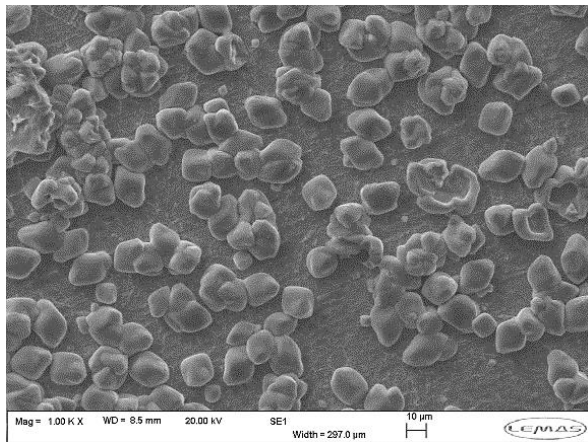
437

438

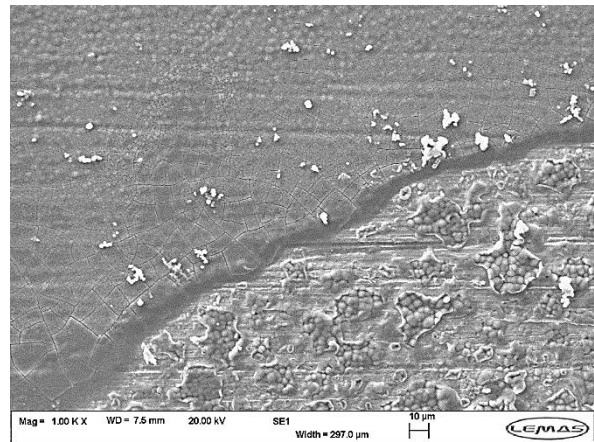
439

440

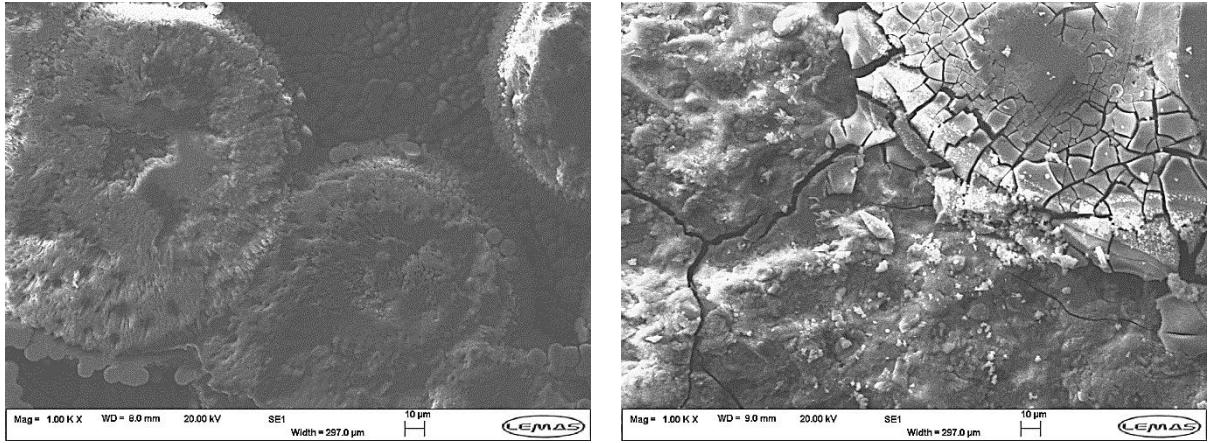
441



(a)



(b)

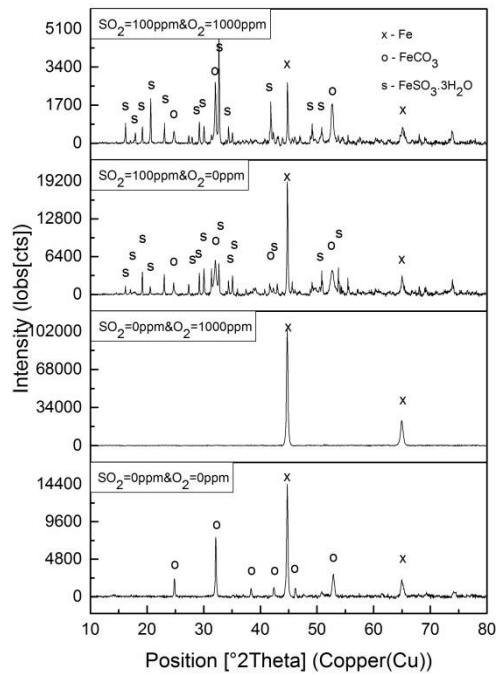


(c)

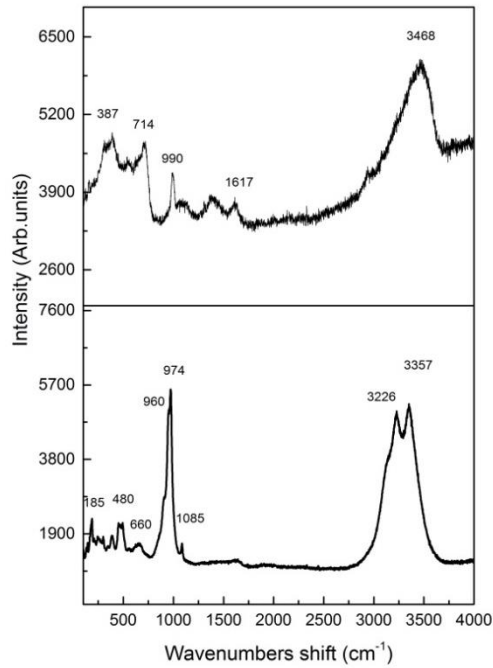
(d)

442 **Figure 5: SEM images of X65 samples exposed to water-saturated supercritical CO<sub>2</sub>**  
 443 **conditions at 80 bar and 35°C containing (a) 0 ppm SO<sub>2</sub> and 0 ppm O<sub>2</sub>; (b) 0 ppm SO<sub>2</sub> and**  
 444 **1000 ppm O<sub>2</sub>; (c) 100 ppm SO<sub>2</sub> and 0 ppm O<sub>2</sub> and (d) 100 ppm SO<sub>2</sub> and 1000 ppm O<sub>2</sub>**  
 445

446



447 **Figure 6: XRD patterns of X65 samples exposed to water-saturated supercritical CO<sub>2</sub>**  
 448 **containing various SO<sub>2</sub> and O<sub>2</sub> at 35°C and 80 bar after 48 h**



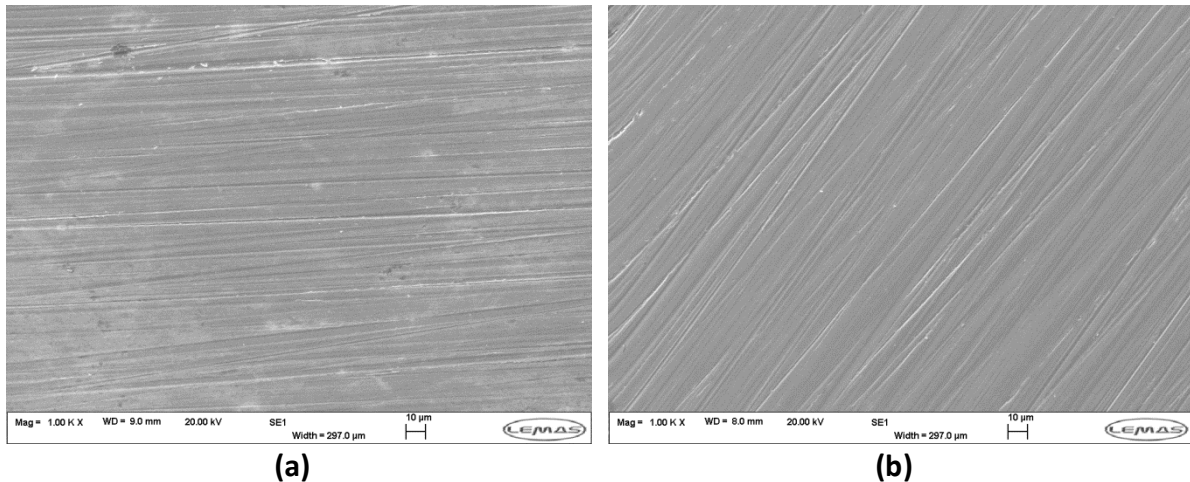
449

450

**Figure 7: Raman spectra of X65 sample exposed to water-saturated supercritical CO<sub>2</sub> containing 100 ppm SO<sub>2</sub> and 1000 ppm O<sub>2</sub> at 35°C and 80 bar after 48 h**

451

452



(a)

(b)

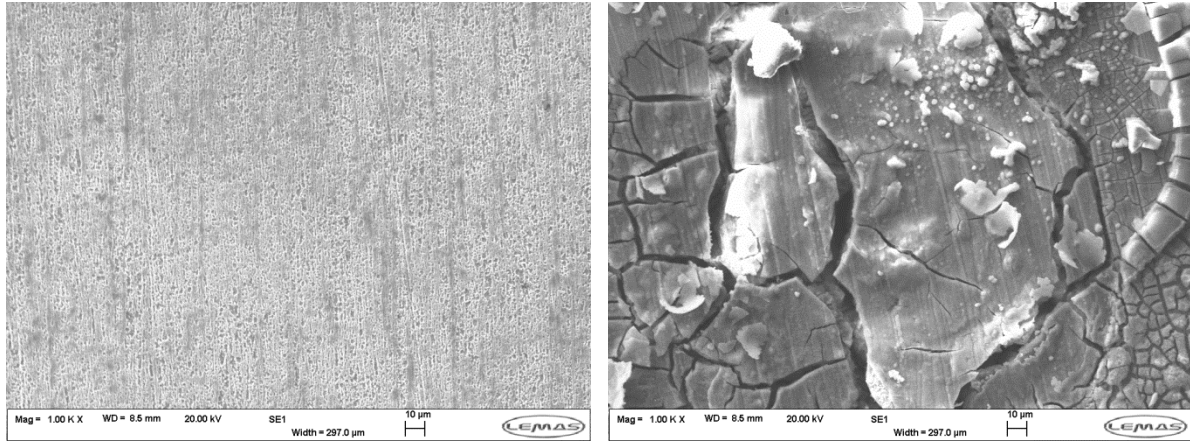
453

**Figure 8: SEM images of 13Cr samples exposed to water-saturated supercritical CO<sub>2</sub> condition with, (a) 0 ppm SO<sub>2</sub> and 0 ppm O<sub>2</sub> and (b) 0 ppm SO<sub>2</sub> and 1000 ppm O<sub>2</sub> after 48 h**

454

455

456



(a)

(b)

457 **Figure 9: SEM images of 13Cr samples exposed to water-saturated supercritical CO<sub>2</sub>**  
458 **condition with (a) 13Cr - 100 ppm SO<sub>2</sub> and 0 ppm O<sub>2</sub>, (b) 13Cr - 100 ppm SO<sub>2</sub> and 1000 ppm**  
459 **O<sub>2</sub> after 48 h**

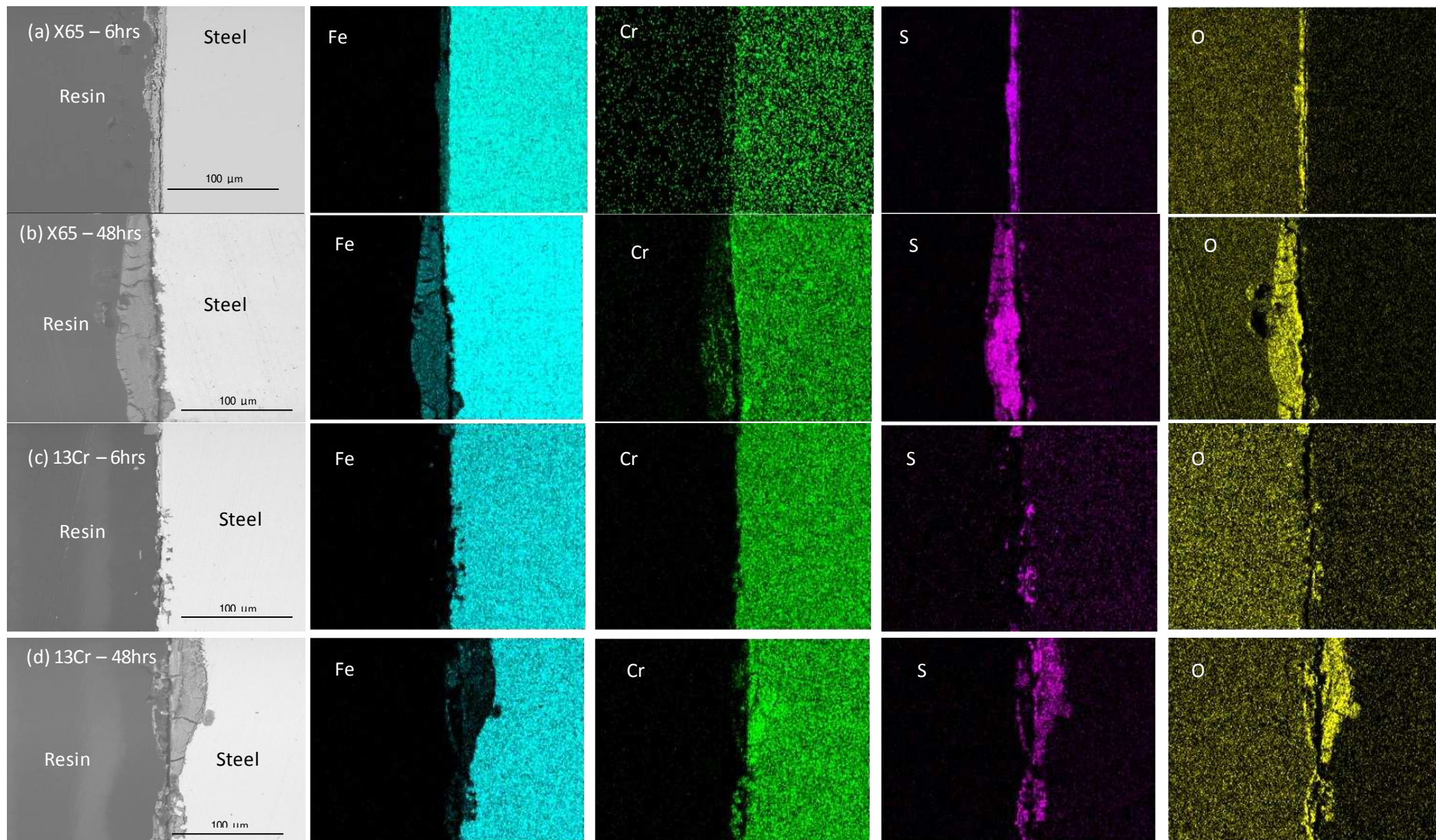
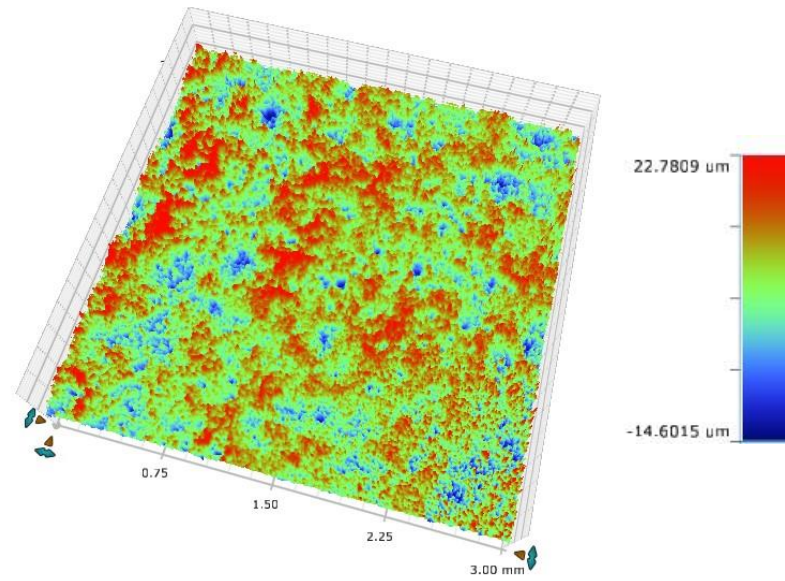
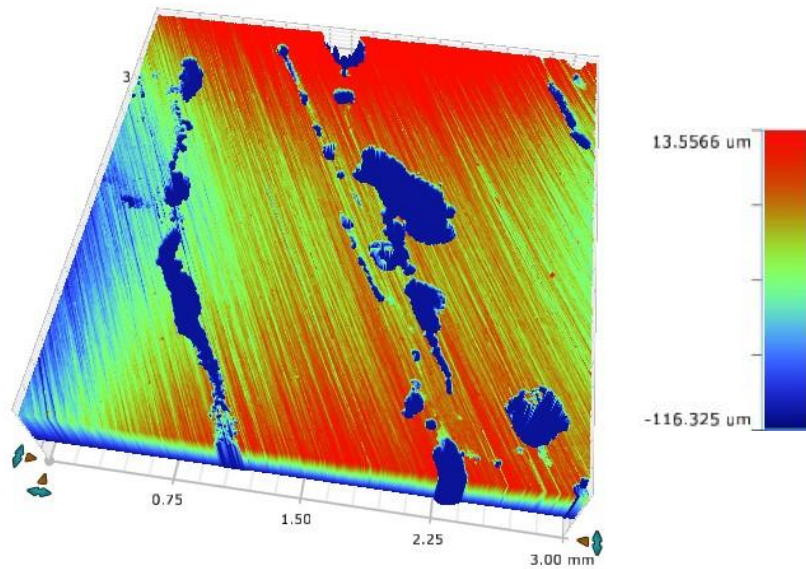


**Figure 10: SEM cross-section images of (a) X65 – 6 hours, (b) X65 – 48 hours, (c) 13Cr – 6 hours and (d) 13Cr – 48 hours samples exposed to water-saturated supercritical CO<sub>2</sub> at 80 bar and 35°C with 100 ppm SO<sub>2</sub> and 1000 ppm O<sub>2</sub>.**



(a)



(b)

Figure 11: Examples of profilometry images (after removal of corrosion products) from (a) X65 and (b) 13Cr after exposure to water-saturated supercritical CO<sub>2</sub> in the presence of 100 ppm SO<sub>2</sub> and 1000 ppm O<sub>2</sub> at 35°C and 80 bar for 48 h

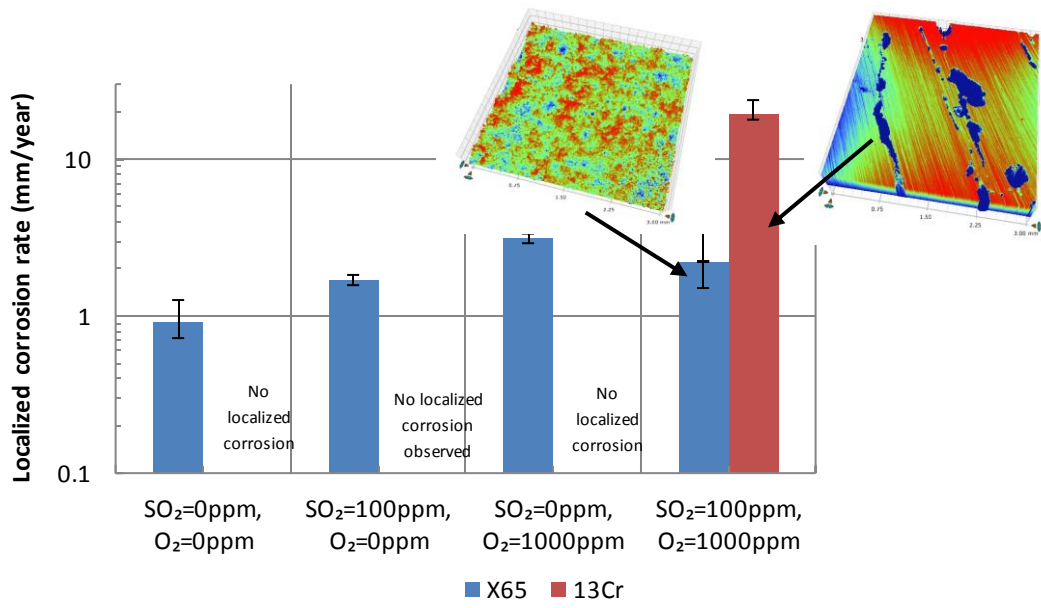


Figure 12: Localized corrosion rates of X65 and 13Cr in water-saturated supercritical CO<sub>2</sub> environments containing varying concentrations of SO<sub>2</sub> and O<sub>2</sub> at 35°C and 80 bar for 48 h

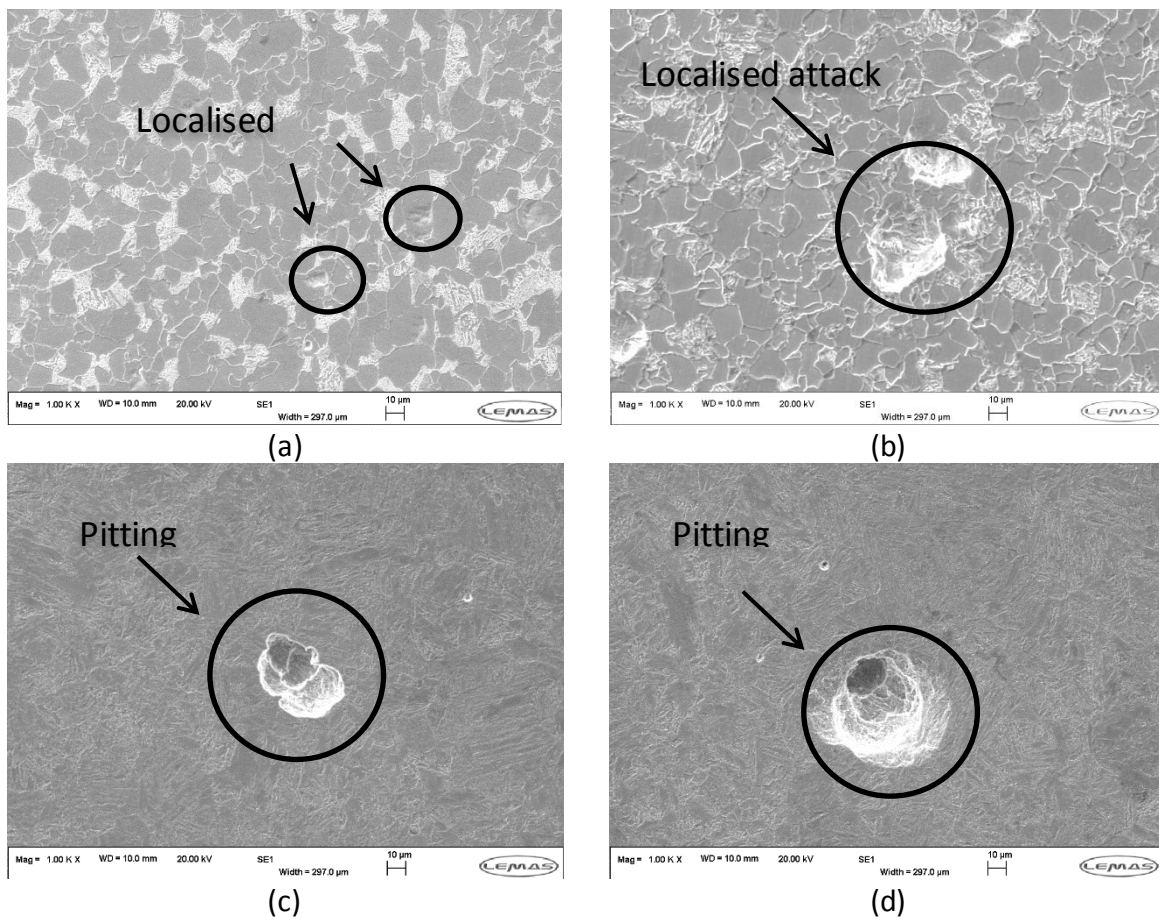
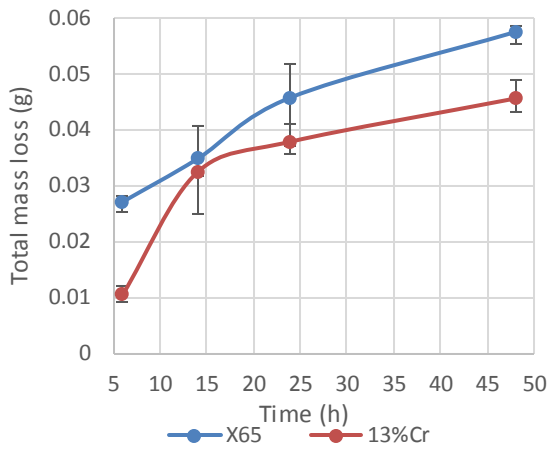
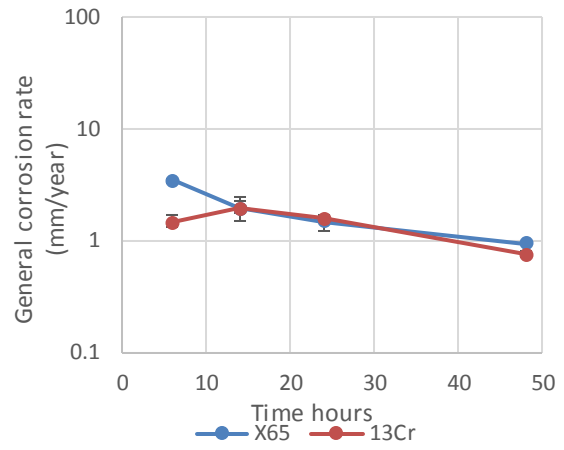


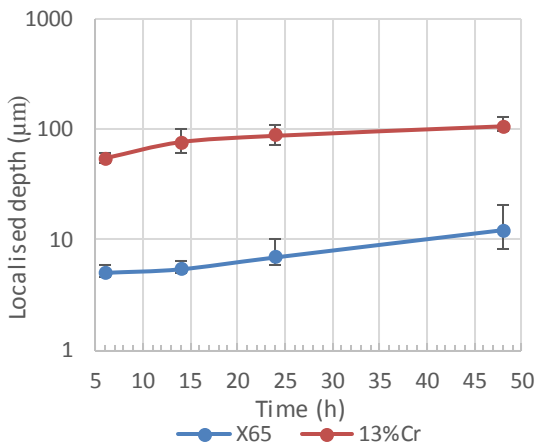
Figure 13: SEM images of samples (after removal of the corrosion products) exposed to water-saturated supercritical CO<sub>2</sub> condition with 100 ppm SO<sub>2</sub> and 1000 ppm O<sub>2</sub> (a) X65 – 6 h, (b) X65 - 48 h, (c) 13Cr – 6 h and (d) 13Cr – 48 h



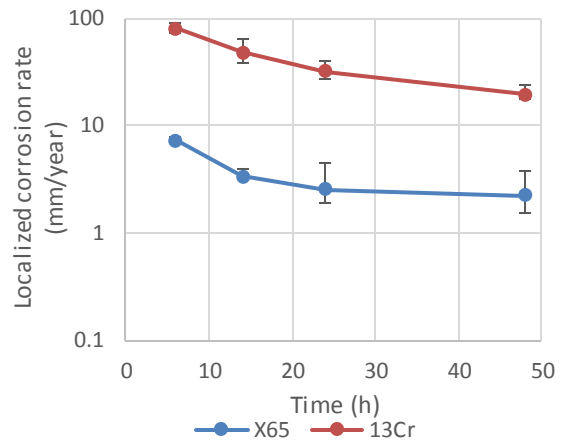
(a)



(b)



(c)



(d)

**Figure 14: (a and b) Total mass loss and general corrosion rates and (c and d) localized depth and localized corrosion rates of X65 and 13Cr in water-saturated supercritical CO<sub>2</sub> in the presence of 100 ppm SO<sub>2</sub> and 1000 ppm O<sub>2</sub> at 80 bar and 35 °C for exposure times of 6, 14, 24 and 48 h**

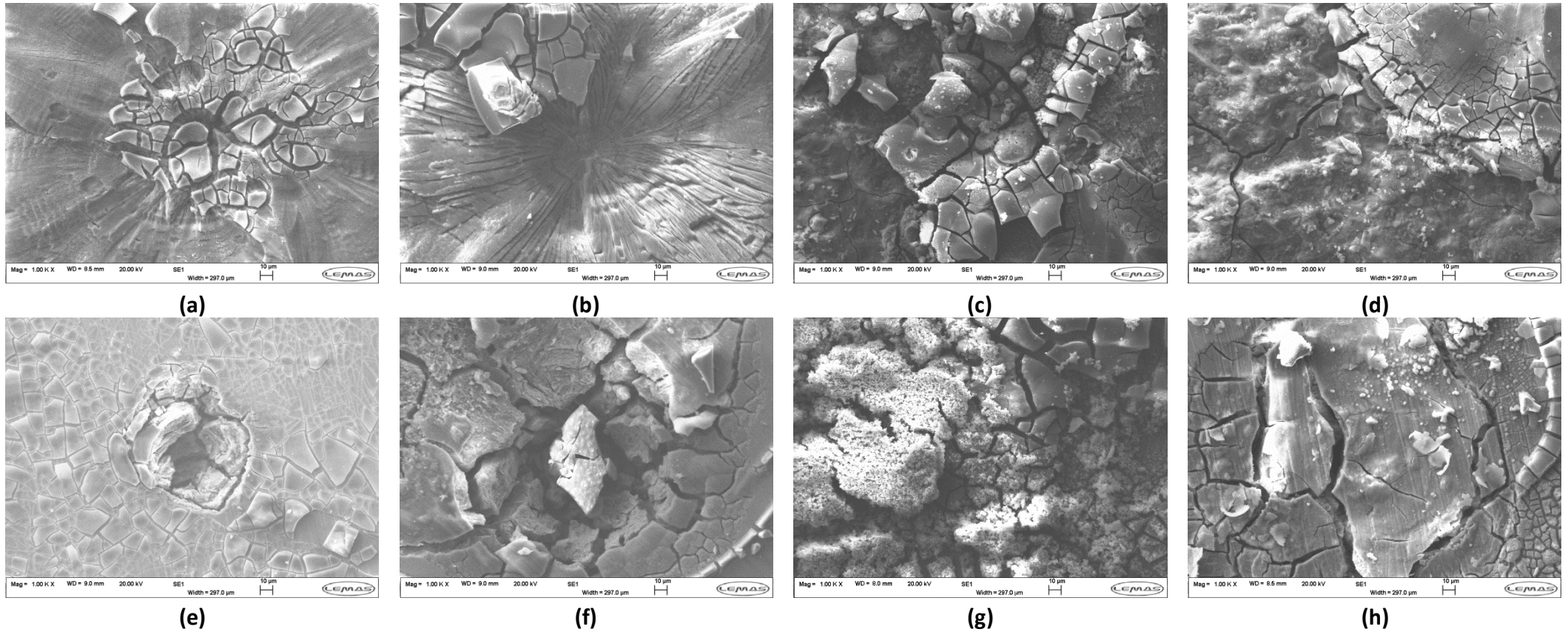


**Figure 15: SEM images of samples exposed to water-saturated supercritical CO<sub>2</sub> with 100 ppm SO<sub>2</sub> and 1000 ppm O<sub>2</sub> (a) X65 – 6 h, (b) X65 – 14 h, (c) X65 – 24 h, (d) X65 – 48 h, (e) 13Cr – 6 h, (f) 13Cr – 14 h, (g) 13Cr – 24 h, and (h) 13Cr – 48 h**